

Structural Transitions and Dynamical Regimes for Directional Locking of Particles Driven Over Periodic Substrates

C. Reichhardt and C.J. Olson Reichhardt

Theoretical Division, Los Alamos National Laboratory, Los Alamos, New Mexico 87545 USA

E-mail: charlesr@cnls.lanl.gov

Abstract. We numerically investigate collective ordering and disordering effects for vortices in type-II superconductors interacting with square and triangular substrate arrays under a dc drive that is slowly rotated with respect to the fixed substrate. A series of directional locking transitions occur as the drive rotates when the particle motion locks to symmetry directions of the substrate, producing a series of steps in the velocity-force curves. The locking transitions coincide with structural transitions between triangular, square, smectic, or disordered particle arrangements, which can be identified using the structure factor. We show that the widths of the locking steps pass through local minima and maxima as a function of the ratio of the number of particles to the number of substrate minima. Unlike a static system, where matching effects occur for simple integer commensuration ratios, our system exhibits dynamical commensuration effects where an integer number of particle chains flow between one-dimensional lines of substrate minima. As the system enters and exits the locking steps, order-disorder transitions in the structure of the moving particle assembly occur. We identify two distinct symmetry locking regimes as a function of substrate strength which produce different locking step characteristics. For weak substrates, all the particles are in motion and a portion of the particles flow through the substrate minima, leading to structural transitions at certain driving angles. For strong substrates, some particles are permanently pinned while the remaining particles flow around them. At the crossover between these two regimes of substrate strength, some or all of the locking steps are destroyed due to the onset of chaotic plastic flow which produces pronounced changes in the transport characteristics. We show that similar effects occur for colloidal particles driven over square and triangular substrate arrays.

PACS numbers: 74.25.Qt,82.70.Dd

1. Introduction

There have been numerous studies of collections of driven particles interacting with periodic substrates in which directional or kinetic locking of the particle motion occurs [1, 2, 3, 4, 5]. Here, some or all of the particles move along a symmetry direction of the substrate even though the external driving force is not applied along the symmetry direction. This effect was first observed in a superconducting vortex system with a square pinning array in [1]. The direction of drive was rotated with respect to the substrate by applying one dc drive F_D^x along a major symmetry axis of the array while gradually increasing a second perpendicular dc drive F_D^y . The initial dc drive was strong enough to cause all the vortices to flow over the substrate so that there were no pinned vortices. As F_D^y increased, the y -component of the response did not increase smoothly as would be expected in the absence of pinning, but instead increased in a series of steps which formed as the vortex motion locked to different symmetry directions of the substrate. For a square substrate lattice, locking steps appear whenever $F_D^y/F_D^x = n/m$, where n and m are integers, giving a devil's staircase structure. Although this initial study was performed for superconducting vortices, in [1] it was suggested that similar effects should occur for other systems of particles moving over periodic substrates at varied drive angles, such as colloidal particles moving over optical substrates. A later study predicted similar effects for the motion of classical charged particles over a two dimensional periodic potential array [2]. The first experimental observation of this type of symmetry locking was obtained for colloidal particles driven at different angles over an optically generated square substrate [3]. The locking, termed kinetic locking in [3], was proposed as a novel fractionation method for separating different colloidal species which could be effective whenever one species locked much more strongly than the other to the symmetry direction of the optical array. Such separation was specifically demonstrated in other experiments with colloidal particles moving over periodic substrates [4]. Following these works, there have been numerous experiments and simulations showing symmetry locking for particles moving on periodic substrates [5, 6, 7, 8, 9, 10, 11, 12, 13, 14, 15, 16, 17, 18, 19, 20], as well as new proposals for achieving a similar effect with nanoparticles [21]. Most of these studies [2, 3, 4, 5, 7, 8, 9, 10, 11, 12, 13, 14, 15, 16, 17, 18, 19, 20] involved noninteracting particles and did not consider collective effects. In the superconducting system studied in [1], the particle-particle interactions are sufficiently long ranged that collective particle interactions play an important role in the response of the system, producing different types of triangular or square orderings. This suggests that there could be a rich variety of collective behaviours and even different types of symmetry locking for particles driven over periodic substrates that have not been explored yet.

In addition to the colloidal work, symmetry locking effects have been further studied for superconducting vortices in numerical simulations [22, 23] and have also been observed experimentally [22, 24, 25, 26]. For systems in which the particles are strongly interacting, dynamical symmetry locking effects can occur even when the particles are moving over a *random* substrate provided that the particle-particle interactions are strong enough to overcome the randomness of the substrate and produce a triangular ordering of the moving particles [27, 28]. The initial triangular ordering of a lattice of strongly interacting vortices results in directional locking steps whenever the direction of the external drive matches one of the lattice vectors of the triangular vortex lattice. Under these conditions, the transverse depinning threshold

for motion perpendicular to the lattice symmetry directions is enhanced. This effect was predicted in theoretical work on the moving vortex Bragg glass where the vortex lattice maintains its triangular ordering [27] and was also observed in numerical simulations for systems with weak random substrates [28]. The appearance of a critical or nonzero transverse depinning threshold due to directional locking has also been predicted to occur for frictional systems of sliding elastic manifolds on periodic surfaces [29, 30, 31]. Vortices and colloids driven over quasicrystalline arrays at varied angles also show directional locking effects where the motion locks to certain orientational degrees of freedom of the lattice even though the substrate has no long-range translational order [32].

Since numerical models of vortex and colloidal systems have proved to be valuable systems for understanding the general behaviour of particles moving over periodic substrates, in this work we use the motion of vortices and colloids to study several aspects of collective effects in symmetry locking that have not been considered previously. The initial study of the symmetry locking effect for a square substrate was performed in the limit where all the vortices were moving [1]. It would be interesting to understand how the locking effects change as the ratio of the external drive to the pinning strength is varied, particularly when a portion of the particles become pinned for stronger substrates. One example of a system exhibiting partial pinning is a superconductor with an applied magnetic field of $B/B_\phi > 1.0$, where B_ϕ is the field at which the number of vortices in the sample equals the number of substrate minima in the sample. If each substrate minima can trap only one vortex, then for $B/B_\phi > 1$, a portion of the vortices occupy interstitial locations between the substrate minima. In order to move under an applied current, these interstitially confined vortices must either flow along the occupied rows of pinning by displacing the pinned vortices, or they can flow through the interstitial regions between the pinning sites [33, 34, 35, 36]. Interstitial vortices, when present, are much more mobile than the pinned vortices and depin at a lower driving threshold than the vortices at the pinning sites [33, 36, 37]. The interstitial vortices may exhibit dynamical locking effects as the direction of the drive is changed; however, it is also possible that for some driving directions the moving interstitial vortices can cause a portion of the vortices at the pinning sites to depin, disrupting or changing the locking effects. The initial symmetry locking study of vortices moving through a square pinning array [1] focused only on fields very near $B/B_\phi = 1.0$, and it is not known how the locking effects would change for higher fields or for varied particle density with a fixed pinning density. It might be expected that the strength of the locking effects would simply decrease for increasing particle density; however, in this work we show that the locking actually undergoes particle density-induced oscillations related to dynamical commensurability effects.

2. Simulation

We model a two-dimensional system with periodic boundary conditions. For the case of superconducting vortices, we consider a sample of size $24\lambda \times 24\lambda$, where length is measured in units of the London penetration depth λ . The motion of an individual vortex evolves according to the overdamped equation

$$\eta \frac{d\mathbf{R}_i}{dt} = \mathbf{F}_i^{vv} + \mathbf{F}_i^p + \mathbf{F}_i^{ext}. \quad (1)$$

Here \mathbf{R}_i is the location of vortex i and η is the damping coefficient $\eta = \phi_0^2 d / 2\pi \xi^2 \rho_N$, where d is the sample thickness, ξ is the superconducting coherence

length, ρ_N is the normal state resistivity, and $\phi_0 = h/2e$ is the flux quantum. The first term on the right is the vortex-vortex interaction force given by $\mathbf{F}_i^{vv} = \sum_{j \neq i}^{N_v} f_0 K_1(R_{ij}/\lambda) \hat{\mathbf{R}}_{ij}$ where K_1 is the modified Bessel function, $f_0 = \phi_0^2/(2\pi\mu_0\lambda^3)$, $R_{ij} = |\mathbf{R}_i - \mathbf{R}_j|$, and $\hat{\mathbf{R}}_{ij} = (\mathbf{R}_i - \mathbf{R}_j)/R_{ij}$. Since the Bessel function diverges at the origin, we place a cutoff on the interaction force at 0.1λ ; in practice, the vortices do not approach each other this closely. The repulsive force falls off exponentially at larger distances so we place a maximum interaction distance cutoff at 6λ to increase the computational efficiency. The periodic substrate is modelled as N_p parabolic potential traps or pinning sites of radius $R_p = 0.3\lambda$ and maximum strength F_p . The vortex-substrate interaction has the form $\mathbf{F}_i^p = \sum_{k=1}^{N_p} (F_p R_{ik}^{(p)}/R_p) \Theta((R_p - R_{ik}^{(p)})/\lambda) \hat{\mathbf{R}}_{ik}^{(p)}$. Here Θ is the Heaviside step function, $R_k^{(p)}$ is the location of pinning site k , $R_{ik}^{(p)} = |\mathbf{R}_i - \mathbf{R}_k^{(p)}|$, and $\hat{\mathbf{R}}_{ik}^{(p)} = (\mathbf{R}_i - \mathbf{R}_k^{(p)})/R_{ik}^{(p)}$. The pinning sites are placed in a triangular or square arrangement.

The initial vortex configurations are obtained by simulated annealing, where we form a high temperature molten state by applying Langevin kicks to the vortices, and slowly cool the sample to $T = 0$. We anneal by decreasing T in increments of $\delta T = 0.002$ with a waiting time of 5000 simulation time steps between increments. After annealing, we apply an external force in the form of a drive applied at an angle that changes very slowly,

$$\mathbf{F}_{ext} = A \sin(\theta(t)) \hat{\mathbf{x}} + A \cos(\theta(t)) \hat{\mathbf{y}} \quad (2)$$

Here the force amplitude is $A = 2.0$, $\theta = \omega t$, and ω is the frequency of rotation, which is taken to be small. The velocity response in the x and y directions can be obtained by measuring the average vortex velocities $\langle V_x \rangle = N_v^{-1} \sum_{i=1}^{N_v} \mathbf{v} \cdot \hat{\mathbf{x}}$ and $\langle V_y \rangle = N_v^{-1} \sum_{i=1}^{N_v} \mathbf{v} \cdot \hat{\mathbf{y}}$. We measure the velocity as a function of the drive angle θ . We focus on the case of low frequencies to avoid any transient effects in the vortex dynamics. We have specifically checked that the simulated annealing time is long enough that the initial vortex configurations do not change for slower annealing rates and that the rotation frequency is small enough that there are no changes in the widths of the directional locking steps for lower values of ω .

For the colloidal simulations we use the same type of overdamped equation of motion and the same form for the pinning substrates. The main difference is the particle-particle interactions, which are still repulsive but have the Yukawa form $\mathbf{F}_i^{vv} = -\sum_{j \neq i}^{N_v} \nabla V(R_{ij}) \hat{\mathbf{R}}_{ij}$ with $V(R_{ij}) = (E_0/R_{ij}) \exp(-\kappa R_{ij})$, where $E_0 = Z^{*2}/4\pi\epsilon\epsilon_0$, ϵ is the solvent dielectric constant, Z^* is the effective charge of each colloid and $1/\kappa$ is the screening length. In this case lengths are measured in units of a_0 and forces in units of $F_0 = E_0/a_0$.

3. Structural Transitions and Directional Locking

In figure 1(a) we show a snapshot of the system for a triangular pinning array at $N_v/N_p = B/B_\phi = 1$ and zero drive. The arrow indicates the initial direction of the applied force, which rotates counterclockwise with time. In figure 1(b) we plot the corresponding structure factor for the vortex positions,

$$S(\mathbf{k}) = \frac{1}{L^2} \sum_{i,j} \exp(i\mathbf{k} \cdot [\mathbf{R}_i(t) - \mathbf{R}_j(t)]). \quad (3)$$

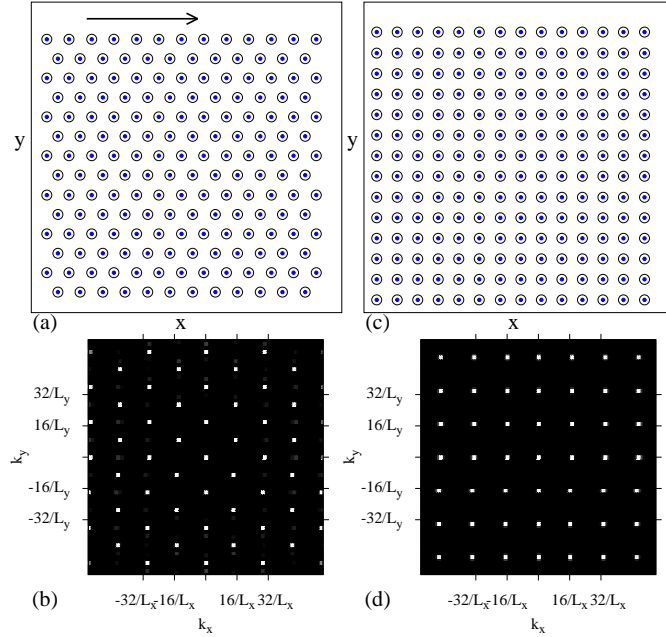


Figure 1. The positions of the pinning sites (large open circles) and vortices (small filled circles) for a triangular pinning array at $B/B_\phi = 1$ and zero drive. The arrow indicates the initial direction of the external drive, which rotates counterclockwise. In this work we consider directional locking for drive angles ranging from $\theta = 0^\circ$ to $\theta = 90^\circ$. (b) The structure factor $S(k)$ for the vortex positions in (a) indicates triangular ordering. (c) The positions of the pinning sites (large open circles) and vortex locations (small filled circles) for a square pinning array at $B/B_\phi = 1$ and zero drive. (d) $S(k)$ from the vortex positions in (c).

Here, six peaks appear which are indicative of the triangular ordering of the vortex lattice. In figure 1(c) we illustrate the nondriven phase for a square pinning array at $B/B_\phi = 1.0$, along with the corresponding structure factor in figure 1(d).

We first consider directional locking on a triangular pinning substrate, which occurs at driving angles $\theta = \tan^{-1}(\sqrt{3}m/(2n+1))$. The dominant locking angles fall at $\theta = 60^\circ$ for $m = 1, n = 0$ and $\theta = 30^\circ$ for $m = 1, n = 1$. We use the notation (m, n) to denote the locking regions. In figure 2(a) we plot V_y and V_x versus θ for a sample with $F_p = 1.85$ at $B/B_\phi = 1.5$. In the absence of pinning, the velocities would follow a smooth sinusoidal curve with V_y starting from zero and reaching a maximum at $\theta = 90^\circ$ when V_x goes to zero. Figure 2(a) shows that in the presence of pinning, both V_y and V_x pass through a series of pronounced steps and jumps. For $\theta < 10^\circ$, the motion is locked in the x -direction with a finite V_x and $V_y = 0.0$. The value of the y component of the driving force at the end of the $(0, 0)$ step when the locking to the x direction is lost is the critical transverse depinning force F_c^{Tr} corresponding to the $(0, 0)$ locking. At the end of the $(0, 0)$ step there is a discontinuous jump in V_y to a finite value which is correlated with a sudden *increase* in V_x . The increase in V_x occurs even though the x component of the driving force is decreasing. Over the range $11^\circ < \theta < 16^\circ$, V_y increases, passing through a small step near $\theta = 14^\circ$. A large

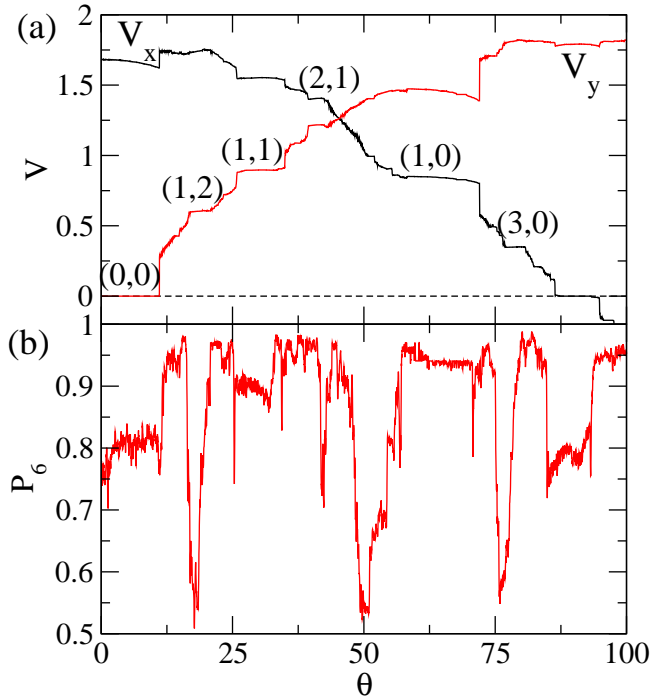


Figure 2. (a) The average velocity V per particle vs drive angle θ for vortices moving on a triangular pinning array with $F_p = 1.85$ at $B/B_\phi = 1.5$. Dark line: V_x ; light line: V_y . Locking steps occur at $\theta = \tan^{-1}(\sqrt{3}m/(2n+1))$, where m, n are integers. Here the locking steps (m, n) at $(0,0)$, $(1,2)$, $(1,1)$, $(2,1)$, $(1,0)$, and $(3,0)$ are highlighted. There is also a locking step at $\theta = 90^\circ$. (b) The corresponding fraction of sixfold coordinated particles P_6 vs θ . Changes in P_6 are correlated with the velocity locking steps in (a).

locking step is centred at $\theta = 30^\circ$ corresponding to the $(1,1)$ locking. A second strong step in both V_x and V_y occurs at $\theta = 60^\circ$ at the $(1,0)$ locking. When the system exits this step, V_y jumps up and V_x jumps down. In figure 2(b) we plot the fraction of sixfold coordinated particles P_6 as a function of θ . Here $P_6 = N_v^{-1} \sum_{i=1}^{N_v} \delta(z_i - 6)$, where the coordination number z_i of each particle is obtained from a Voronoi construction. In the absence of pinning, $P_6 = 1.0$ when the vortices form a triangular lattice. On the $(0,0)$ step, $P_6 = 0.8$, indicating that the system does not have complete triangular ordering and that some dislocations must be present. Along the $(1,1)$ step, $P_6 = 0.9$, but P_6 dips at the start and the end of the step. For the first half of the $(1,2)$ step, P_6 has a low value, and then for the second half of the step P_6 increases.

To better characterize the different vortex structures in the locking regimes, in figure 3(a) we plot the vortex positions on the $(0,0)$ step for the system in figure 2, and in figure 3(b) we show the corresponding $S(k)$. Here the particles are moving in one-dimensional channels along the pinning rows in the x -direction. $S(k)$ has smectic features with well spaced peaks along the k_y -axis indicating that periodic spacing of the particles along the y direction is induced by the underlying rows of pinning. Particles in adjacent rows can slip past each other along the x direction. In this regime, $P_6 = 0.8$ due to the formation of aligned dislocations between adjacent

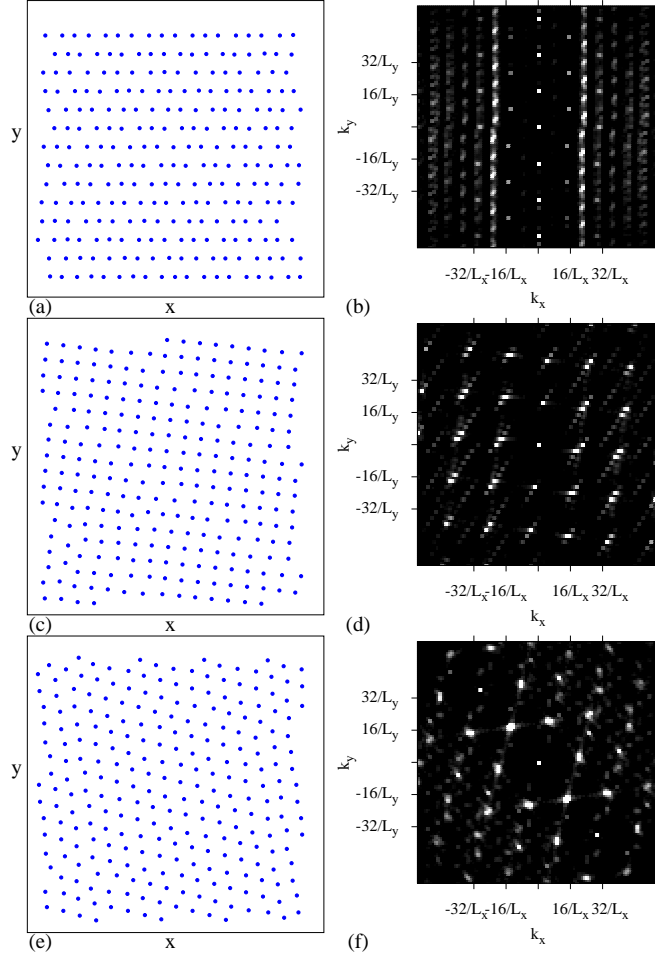


Figure 3. The vortex positions (a,c,e) and corresponding $S(k)$ (b,d,f) for the triangular pinning system in figure 2. (a,b) The smectic structure along the (0,0) step. (c,d) Square lattice formation on the (1,2) step. (e,f) Partial triangular ordering in a non-step region at $\theta = 36^\circ$.

rows. Similar smectic ordering has previously been observed for vortices moving over random pinning arrays [38, 39, 40, 41] and is associated with a transverse depinning barrier [38, 39, 42]. For vortices moving over pinning arrays with driving applied only in the x -direction, moving smectic phases are also possible at finite temperature [43, 44]. In figure 3(a), the smectic ordering occurs when all the vortices are confined to move only along the pinning rows and not between the rows of pinning. Since $B/B_\phi > 1.0$, this means that the vortex lattice spacing in the x direction along the pinning rows must be smaller than the lattice spacing in the y direction transverse to the pinning rows, resulting in an effectively anisotropic interaction between the vortices. Additionally, certain moving channels may contain more vortices than other moving channels, creating dislocations in the vortex lattice. Along the (1,1) step, the system has a smectic ordering similar to that shown in figure 3(a,b) but tilted by 30° with respect to the x axis.

Figure 3(c,d) illustrates the vortex positions and $S(k)$ on the (1,2) locking step. In this case the vortex lattice has square symmetry with some disordered regions which produce some smearing in $S(k)$. The formation of the square ordering is what causes the drop in P_6 on the (1,2) step shown in figure 2(b). The Voronoi construction we use to determine the particle coordination numbers z_i can accurately identify triangular ordering but is not well suited for measuring slightly disordered square ordering such as that found on the (1,2) step. As a result, P_6 shows large fluctuations on the (1,2) step even though the $S(k)$ measurement indicates the presence of a consistent square ordering throughout the step.

In figure 3(e,f) we show the vortex positions and $S(k)$ for $\theta = 36^\circ$, a non-step region with $P_6 = 0.95$. The system has triangular ordering as indicated by the sixfold peaks in $S(k)$. Typically the vortex channeling effect is lost in the non-step regions. For sufficiently weak pinning the vortex-vortex interactions dominate over the vortex-pin interactions and the vortices form a mildly disordered triangular lattice, resulting in large values of P_6 .

Figure 2(a) shows a prominent (1,0) locking step at $\theta = 60^\circ$. Along the step, V_y decreases with increasing θ until at $\theta = 70.1^\circ$ there is a sharp jump up in V_y along with a sharp jump down in V_x at the end of the locking step. This shows that directional locking can induce *negative differential conductivity*, where the driven particles actually move more slowly in the direction of drive when the external driving force is increased. Negative differential conductivity has been observed in simulations and experiments for vortices driven in a fixed direction over periodic pinning arrays [36, 45]. The negative differential conductivity effect which we observe here for triangular pinning did not appear in previous simulations which considered only square pinning [1]. More recently a study with two crossed channels showed that a phase locking state could be realized that has velocity-force curves very similar to those in figure 2(a) and that also exhibits negative differential conductivity [46].

In figure 2(b), the (1,0) locking step has dips in P_6 at the start and end of the step, while along the step $P_6 = 0.945$. The dips are caused by the sudden disordering of the particles at the transition into and out of the locked regime, and are associated with a strongly anisotropic vortex lattice structure. In figure 4(a,b) we show the particle positions and $S(k)$ for $\theta = 60^\circ$ on the (1,0) step. The particles again form one-dimensional channels and move along the pinning rows. There are some dislocations present in the vortex lattice which result in smectic ordering; however, there is a considerably larger amount of ordering in the direction transverse to the locking direction than along the locking direction, causing the amount of smearing in $S(k)$ to be less than that observed for the (0,0) step. Figure 4(c,d) illustrates the system at the dip in P_6 right at the end of the (1,0) locking step. The lattice structure is disordered, producing a ringlike structure in $S(k)$. Smearred sixfold peaks remain visible in $S(k)$ due to the anisotropic nature of the liquidlike structure.

Figure 2(a) shows that the (3,0) locking step is accompanied by a strong dip in P_6 . Along this step a square vortex lattice forms which is similar to the one illustrated for the (1,2) locking step in figure 3(c,d). There is another locking region centred at $\theta = 90^\circ$ where $V_x = 0.0$ and V_y shows a cusp feature. Along this step $P_6 = 0.78$, and figure 4(e,f) shows that a distorted square lattice appears. As θ increases above $\theta = 90^\circ$, the system cycles back through the same transitions.

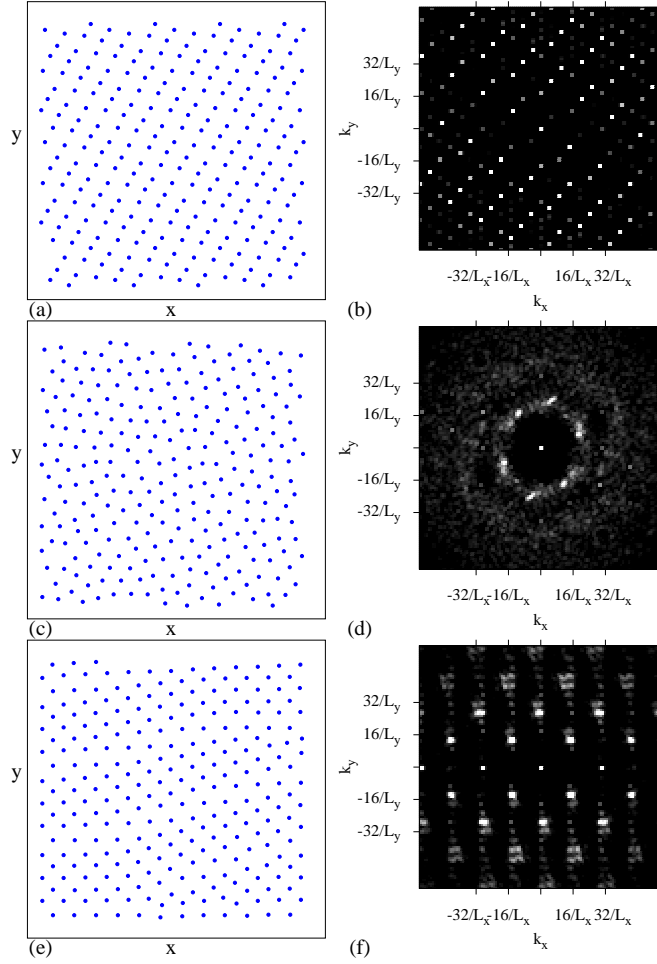


Figure 4. The vortex positions (a,c,e) and corresponding $S(k)$ (b,d,f) for the triangular pinning system in figure 2. (a,b) The smectic structure on the $(1,0)$ step. (c,d) An anisotropic liquid at the transition out of the $(1,0)$ step. (e,f) A distorted square lattice at the locking regime for $\theta = 90^\circ$

4. Density Dependence and Dynamic Commensuration Effects

We next consider the effect of particle density on the directional locking. In figure 5(a) we plot V_y for the same triangular pinning system from figure 2 with $F_p = 1.85$ for different vortex densities $B/B_\phi = 0.852, 1.26, 1.5, 2.0, 2.78,$ and 4.07 . As the vortex density increases, the smaller steps become narrower and more difficult to resolve; however, the steps at $(0,0)$, $(1,1)$, $(1,0)$, and $\theta = 90^\circ$ remain clearly visible. Different steps respond differently to changes in θ . For example, for $B/B_\phi < 2.0$ the $(0,0)$ and $(1,0)$ steps are present but at $B/B_\phi = 2.0$ these steps are lost. In contrast, the step at $(1,1)$ is present at all the values of B/B_ϕ .

The $(0,0)$ and $(1,0)$ steps reappear for $B/B_\phi \geq 2.78$ and grow in width with increasing vortex density up to $B/B_\phi = 4.07$. Figure 5(b) shows a blowup of the region around the $(0,0)$ step indicating that at $B/B_\phi = 2.0$ the width of the $(0,0)$

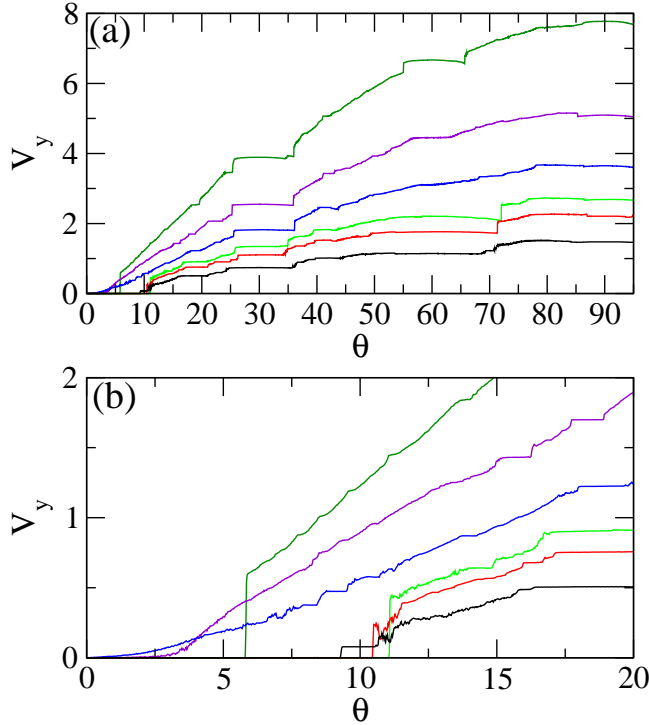


Figure 5. (a) Vortex velocities V_y vs θ for a triangular pinning array with $F_p = 1.85$ at $B/B_\phi = 0.852, 1.26, 1.5, 2.0, 2.78,$ and 4.07 , from bottom right to top right. The velocities are normalized by B_ϕ . (b) A blowup of panel (a) in the region near the $(0,0)$ step showing that the width of the $(0,0)$ step decreases to zero at $B/B_\phi = 2.0$ and increases again for $B/B_\phi = 4.07$

step drops to zero but that at $B/B_\phi = 4.07$ the step reappears, producing a crossing in the V_y versus θ curves. In figure 6 we plot the width F_c^{Tr} of the $(0,0)$ step versus B/B_ϕ , where F_c^{Tr} is defined as $F_c^{Tr} = A \cos(\theta)$, the y component of the force at which the step disappears. For low B/B_ϕ , F_c^{Tr} is large since the system is in the single particle limit when the vortex-vortex interactions are weak. As B/B_ϕ increases, F_c^{Tr} decreases until it reaches a local minimum at $B/B_\phi = 0.75$. This is followed by a local maximum in F_c^{Tr} at $B/B_\phi = 1.4$, after which F_c^{Tr} decreases nearly to zero for $1.8 < B/B_\phi < 2.4$. A broad maximum in F_c^{Tr} appears for $3.0 < B/B_\phi < 5.5$ before F_c^{Tr} drops again at higher B/B_ϕ . This nonmonotonic behaviour of F_c^{Tr} contrasts with the critical depinning force observed in a system with random pinning, which monotonically decreases to a saturation level with increasing vortex density. In recent studies of directional locking for vortices moving over quasicrystalline pinning arrays [32], a nonmonotonic behaviour of the width of the first locking step was observed as a function of B/B_ϕ . In the quasicrystalline case, the width of the step never drops completely to zero; however, a broad local minimum occurs at $B/B_\phi = 1.6$ and a broad peak appears for $1.6 < B/B_\phi < 4.0$, similar to the features shown in figure 6.

In figure 7 we illustrate the vortex positions and $S(k)$ at different vortex densities for the system in figure 6 along the $(0,0)$ step. At $B/B_\phi = 0.74$, figure 7(a) shows that a disordered triangular lattice forms. For lower fillings $B/B_\phi < 0.74$, the ordering

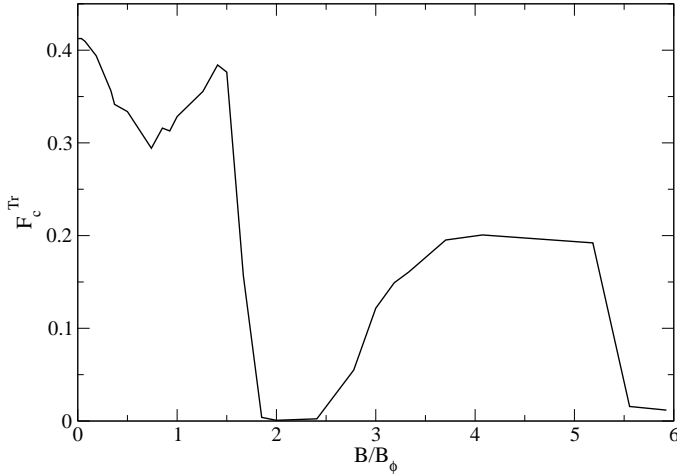


Figure 6. The width F_c^{Tr} of the $(0,0)$ step vs B/B_ϕ for the system in figure 5 with triangular pinning. The width is defined as the force component in the y -direction, $F_c^{Tr} = A \cos(\theta)$. A series of minima and maxima appear that are not simply related to the commensuration effects expected at integer multiples of B/B_ϕ .

becomes more smectic-like as the vortex-vortex interactions are reduced in strength. Smectic ordering also appears close to the peak in F_c^{Tr} at $B/B_\phi = 1.5$, as shown in figure 3(a,b). In the region where F_c^{Tr} drops to zero, the lattice is disordered and $S(k)$ has a ringlike structure, as shown in figure 7(c,d) for $B/B_\phi = 2.037$. There is a tendency for some vortices to form stripe-like structures aligned with the x direction, generating weak peaks in $S(k)$ along the k_y -axis and making the liquidlike structure anisotropic. At $B/B_\phi = 4.074$, near the middle of the broad peak in F_c^{Tr} in figure 6, figure 7(e,f) indicates that the lattice has smectic ordering, while at $B/B_\phi = 5.92$ where F_c^{Tr} drops again, figure 7(g,h) shows that the lattice is disordered with some partial x direction alignment. For $3.8 < B/B_\phi < 5.0$ the vortex lattice has smectic structure while at vortex densities where F_c^{Tr} is low or zero, the vortex lattice is disordered or nematic.

In recent work on the directional locking of vortices moving over quasicrystalline arrays, for values of B/B_ϕ where F_c^{Tr} is enhanced, the vortices have smectic ordering, while for higher B/B_ϕ where the value of F_c^{Tr} drops, the system becomes partially disordered [6]. This is very similar to what we observe for the triangular pinning arrays, as shown in figure 6. In the quasicrystalline array system, square vortex lattices form at fillings where F_c^{Tr} passes through a local minimum but remains finite. At the local minimum in F_c^{Tr} that we observe in figure 6 at $B/B_\phi = 0.74$, the vortex lattice is not square but it does have a distorted triangular ordering, as shown in figure 7(a,b). We note that the dynamical ordering which occurs just above a critical transverse depinning force differs from the dynamical structure that forms just above the longitudinal depinning force. In the case of the transverse depinning, the vortices are already moving and may form a dynamically ordered configuration even before transverse depinning occurs. In contrast, for the longitudinal depinning, the vortices start from a pinned state. For longitudinal depinning, peaks in the critical current occur at matching fields $B/B_\phi = n$ and fractional matching fields m/n , where m and

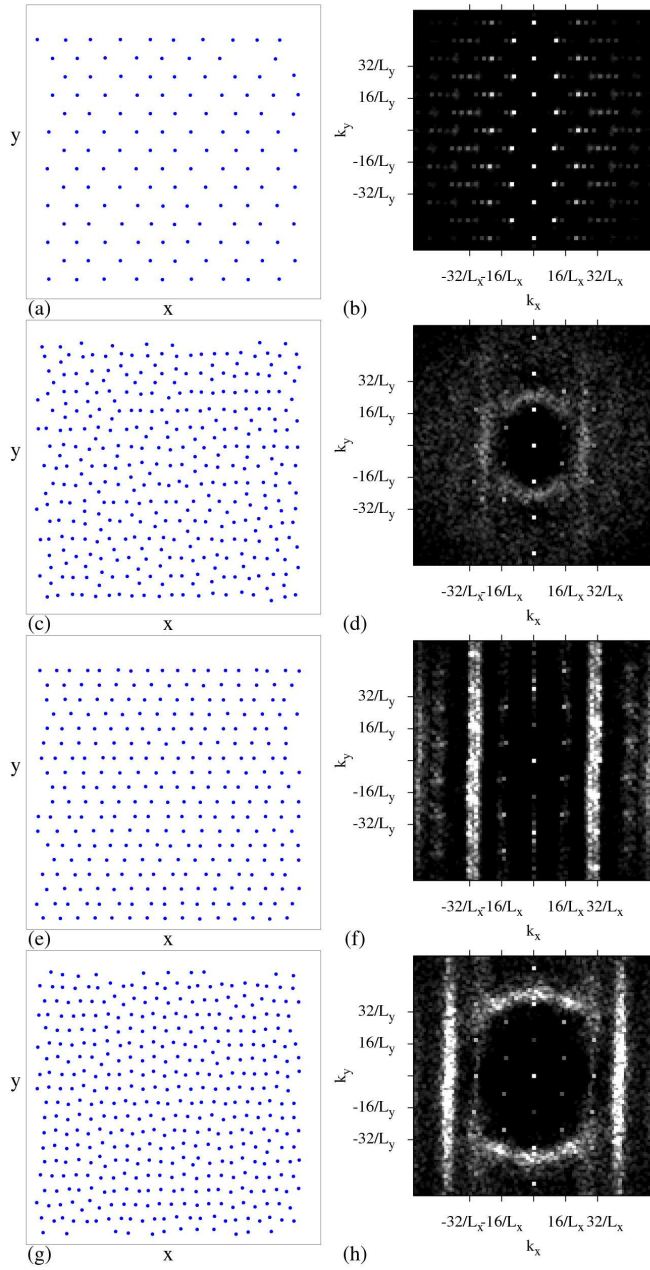


Figure 7. The vortex positions (a,c,e,g) and corresponding $S(k)$ (b,d,f,h) for the triangular pinning system from figure 6 with $F_p = 1.85$ along the $(0,0)$ step. (a,b) $B/B_\phi = 0.74$. (c,d) $B/B_\phi = 2.037$. (e,f) $B/B_\phi = 4.074$. (g,h) $B/B_\phi = 5.92$.

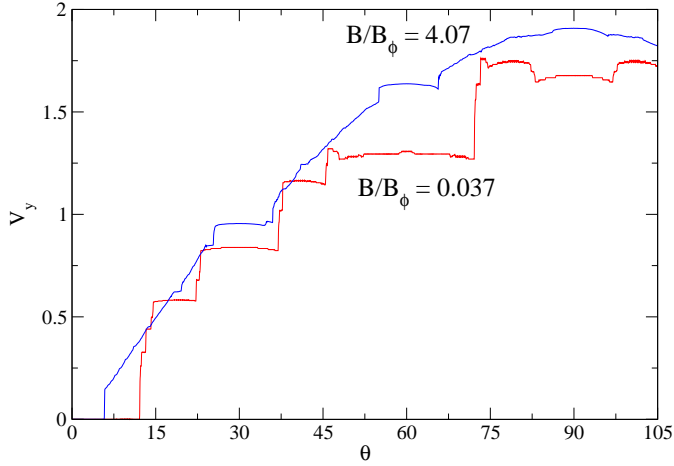


Figure 8. V_y vs θ for the triangular pinning system in figure 5 showing a comparison between the low density, single particle behaviour limit $B/B_\phi = 0.037$ (lower line) and the high density, strongly collective behaviour at $B/B_\phi = 4.07$ (upper line). In the noninteracting limit the particles jump directly from one locking step to another and show no unlocked phases.

n are integers [33, 34, 35, 47]. Figure 6 shows that the peaks in the transverse critical current F_c^{Tr} do not fall at integer matching fields or fractional matching fields, so the local maxima and minima must arise due to some other type of commensuration effect and not due to simple matching between the number of vortices and the number of pinning sites.

At low vortex densities the system acts in the single particle limit and the vortices jump from one locking step to another with no unlocked regions between the steps. At higher densities, unlocked regions of disordered collective flow appear between the steps. A comparison between the low and high density behaviour appears in figure 8, which shows V_y versus θ for $B/B_\phi = 0.037$ and $B/B_\phi = 4.07$. In the unlocked regions, the vortex-vortex interactions are strong enough to permit the vortices to form a triangular lattice. It is the strong vortex-vortex interactions that destroy the higher order steps at the higher densities.

In studies of vortex matter confined to narrow channels, the critical current or depinning force oscillates as a function of vortex density depending on how many rows of vortices can fit inside the channel [48, 49]. More recent studies of two-dimensional periodic pinning arrays show a dynamical commensuration effect that occurs in the limit where the vortices at the pinning sites remain pinned but the number of interstitial vortices flowing through interstitial regions increases with B/B_ϕ [37]. In this case the transverse depinning force F_c^{Tr} exhibits local minima and maxima as a function of B/B_ϕ . At each local maximum, an integer number n of vortex rows fit between the pinned vortices and the vortex trajectories are highly ordered. As long as this integer number of rows can be maintained, F_c^{Tr} remains high, but eventually a buckling instability occurs and produces a disordered moving vortex structure which has a low F_c^{Tr} . As B/B_ϕ increases further, a new ordered vortex state with $n + 1$ rows of moving vortices forms and F_c^{Tr} increases again. The oscillations in F_c^{Tr} shown in figure 6 are very similar in nature to this effect; however, a key difference is that there are no pinned vortices in the rotating drive system. Along the $(0, 0)$ step, all of

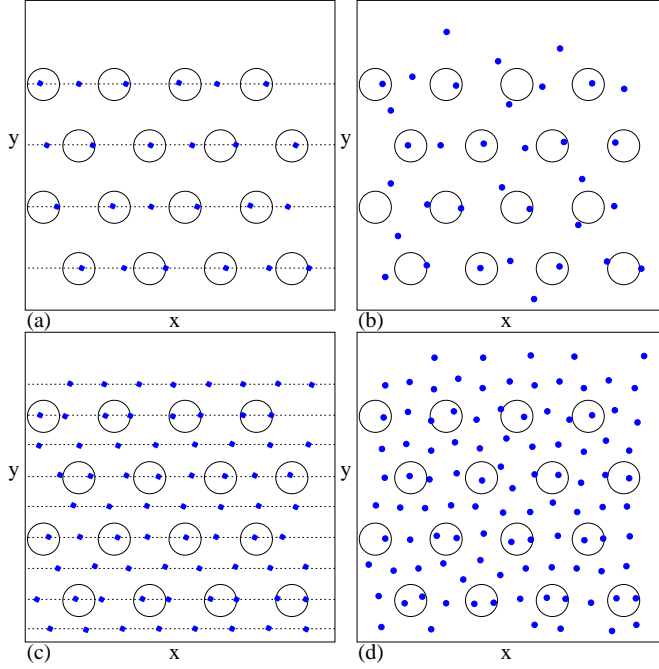


Figure 9. The positions of the pinning sites (large open circles) and vortices (small filled circles) in a portion of the sample for a triangular pinning array along the $(0, 0)$ step for the system in figure 6. (a) $B/B_\phi = 1.5$. The dashed lines indicate the motion of the vortices in one-dimensional channels aligned with the pinning rows. (b) $B/B_\phi = 2.037$, a filling at which $F_c^{Tr} = 0$ in figure 6. Here the one-dimensional channel structure shown in panel (a) is lost. (c) $B/B_\phi = 4.07$, where there are one-dimensional channels of motion both along and between the pinning sites, as indicated by the dashed lines. (d) $B/B_\phi = 5.93$, where F_c^{Tr} is small. The one-dimensional channel structures are lost.

the vortices are moving and some of the vortices are sliding over rows of pinning sites. The remaining vortices slide through the interstitial regions between rows of pinning sites. When an integer number of interstitial sliding rows fits between adjacent rows of vortices sliding over the pinning sites, the structure of the vortex lattice is smectic and there is a local maximum in F_c^{Tr} . At other values of B/B_ϕ where an integer number of interstitial sliding rows is unable to form, the vortex lattice is more disordered and F_c^{Tr} is low or zero. We illustrate this effect in figure 9 where we show the locations of the vortices and pinning sites for different values of B/B_ϕ on the $(0, 0)$ step. Near the local maximum in F_c^{Tr} at $B/B_\phi = 1.5$, figure 9(a) indicates that the vortices flow in one-dimensional channels along the pinning rows and that there are no vortices flowing in the interstitial regions between rows of pinning. At $B/B_\phi = 2.037$, figure 9(b) shows that the vortices are no longer aligned with the pinning rows and that some vortices are flowing through the interstitial regions. Near another local maximum in F_c^{Tr} at $B/B_\phi = 4.07$, we show in figure 9(c) that all of the vortices are flowing in one-dimensional rows and that half of the rows pass through pinning sites while the other half of the rows pass through interstitial regions. At $B/B_\phi = 5.93$, near a local minimum in F_c^{Tr} , figure 9(d) illustrates that the one-dimensional channel structure is lost. We expect that for even higher values of B/B_ϕ , additional local maxima in

F_c^{Tr} will occur for fields at which two, three, or higher integer numbers of rows of vortices can be accommodated in the interstitial regions. This same mechanism of the formation of integer numbers of ordered one-dimensional flowing channels also produces the local minima and maxima in the transverse critical force F_c^{Tr} found for quasicrystalline pinning arrays in [32]. In the quasicrystalline system, the existence of orientational order is sufficient to permit the formation of ordered channels of flow, and translational order is not required. Systems with random pinning substrates exhibit no oscillations in F_c^{Tr} as a function of field since these substrates lack long-range orientational order. We thus expect that any periodic or quasiperiodic pinning substrate which has orientational order will produce oscillations in the transverse depinning force as a function of particle density. Similar oscillations of the widths of the higher order locking steps with increasing field should also occur; however, since the spacing between the one-dimensional channels of particles flowing along the pinning sites will vary from step to step, the particle densities at which the local minima or maxima in step width occur may be different than the densities at which maxima and minima of F_c^{Tr} for the (0,0) step occur.

5. Square Pinning Array

The same general behaviour found for the triangular pinning array also occurs for vortices moving over square pinning arrays. In figure 10(a) we plot V_y versus drive angle θ for a sample containing a square pinning array with $F_p = 1.5$ for $B/B_\phi = 0.2, 1.5,$ and 4.0 . In the square array, locking steps appear when $\theta = \tan^{-1}(m/n)$ with m and n integers, and in the figure we highlight steps with $(m,n) = (0,1), (1,3), (1,2), (1,1), (2,1), (3,1),$ and $(1,0)$. The most prominent steps fall at (0,1) for $\theta = 0^\circ$ and (1,1) for $\theta = 45^\circ$. At $B/B_\phi = 4.0$, many of the higher order steps are very small or or missing and the (1,1) step is much reduced in size while the (1,2) and (2,1) steps remain prominent. In figure 10(b) we plot the width of the (0,1) step F_c^{Tr} vs B/B_ϕ . The behaviour of F_c^{Tr} is very similar to that shown for the triangular pinning array in figure 6. For the square array, local minima in F_c^{Tr} appear at $B/B_\phi = 0.6, 2.0,$ and 5.5 . At the local maxima of F_c^{Tr} , we find the same one-dimensional channeling effects described in the previous section for the triangular pinning arrays. The structure of the vortex lattice on the steps in the square pinning array system is also similar to that found for the triangular arrays, as illustrated in figure 11. For example, a smectic structure appears at $B/B_\phi = 1.5$ on the (0,1) step, shown in figure 11(a,b). One distinction is that the square pinning array system shows a much larger number of locking steps where the vortices form a square moving lattice structure, such as that illustrated for the (1,2) step at $B/B_\phi = 1.5$ in figure 11(c,d).

6. Substrate Strength and Different Locking Regimes

We next consider the effect of substrate strength on the locking regimes for a system with a triangular pinning lattice at fixed $B/B_\phi = 1.11$. In figure 12 we plot V_y versus θ for samples with $F_p = 0.25, 0.5, 1.0,$ and 1.5 . The step widths grow with increasing F_p . A similar effect was observed for locking on square pinning arrays in previous work [1]. As the substrate strength becomes very large, we observe a new phenomenon where the locking effects become reduced. The plot of V_y versus θ for $F_p = 2.35$ in figure 13(a) shows that although the (0,0) and the (1,0) locking steps are present, all of the remaining steps are gone and are replaced by a strongly fluctuating

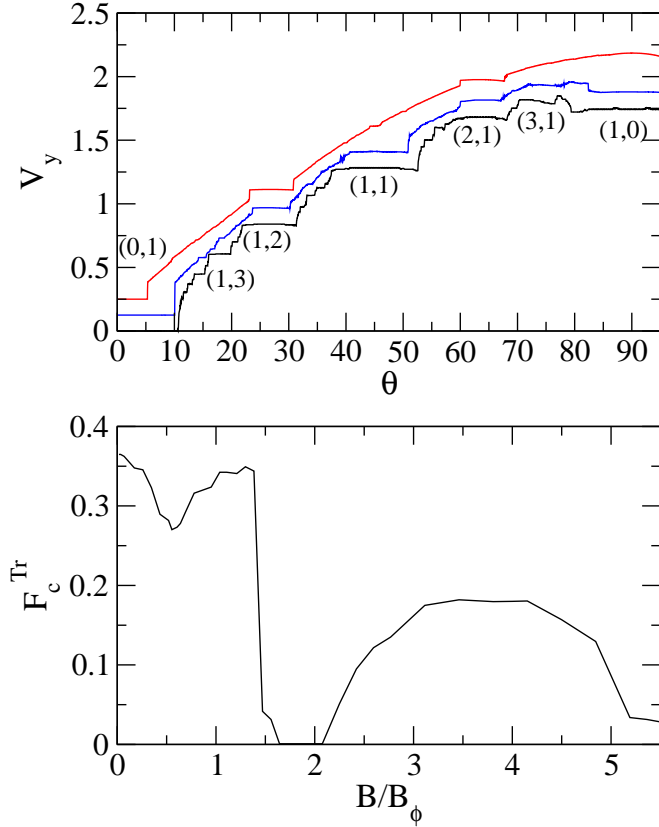


Figure 10. (a) V_y vs θ for a sample with a square pinning array at $F_p = 1.5$ for $B/B_\phi = 0.2, 1.5,$ and 4.0 (from bottom to top). Locking steps occur at $\theta = \tan^{-1}(m/n)$ where m and n are integers. The steps at $(m, n) = (0, 1), (1, 3), (1, 2), (1, 1), (2, 1), (3, 1),$ and $(1, 0)$ are marked. The $B/B_\phi = 0.2$ and $B/B_\phi = 1.5$ curves have been shifted up for clarity. (b) The width of the first step given by F_c^{Tr} , the value of the force component in the y direction, vs B/B_ϕ for the same system.

regime. Some directional guidance effects still occur within this strongly fluctuating regime, as shown by the dip in V_y appearing at $\theta = 90^\circ$ and the shoulder feature near $\theta = 36^\circ$. In the non-step regions, the flow is strongly disordered. The trajectories of the particles do not fall into ordered channels but mix strongly, and vortices become pinned and depinned at random. Although ordered flow occurs along the $(0, 0)$ and $(1, 0)$ steps, it differs from the ordered flow found at the lower pinning forces shown in figure 12. We find that collective effects between the particles begin to dominate the behaviour once $F_p > 2.0$. In a system with a vortex density low enough to fall into the single particle behaviour limit, all of the vortices are immobilized for $F_p > 2.0$ since the pinning strength exceeds the magnitude of the driving force, $F_p > A$. For all of the values of F_p shown in figure 12, we have $F_p < A$ and there are no pinned vortices; instead, all of the vortices flow along or between the pinning sites. On the locking steps at $F_p = 2.35$, motion occurs in the form of a pulse of depinned vortices which passes through a background of pinned vortices. Each vortex spends part of the

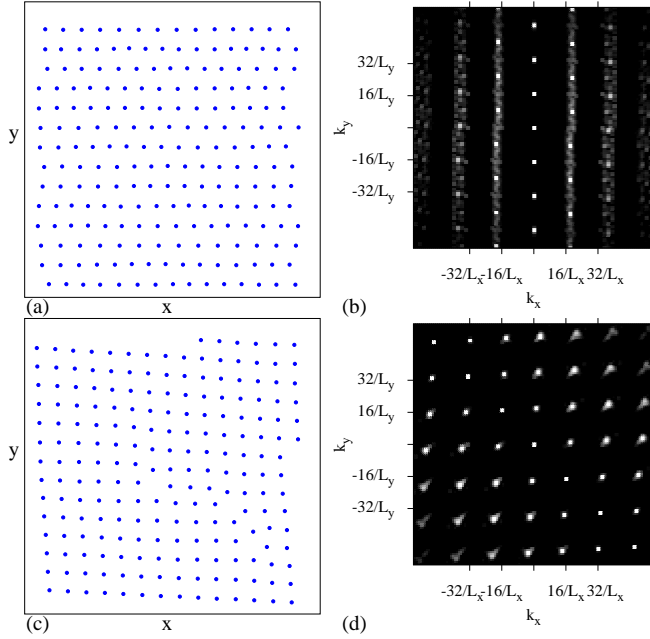


Figure 11. The vortex positions (a,c) and corresponding $S(k)$ (b,d) for the square pinning system from figure 10 with $F_p = 1.5$ at $B/B_\phi = 1.5$. (a,b) The (0, 1) step. (c,d) The (1, 2) step.

time pinned and part of the time moving, and there are always some pinned vortices present, but the identity of the the pinned vortices is constantly changing. This is why V_y along the (1,0) step for $F_p = 2.35$ is nearly a factor of 3 lower than V_y along the (1,0) step for $F_p = 1.5$, where the vortices move continuously and are never pinned. A similar soliton or incommensurate flow of vortices along rows of pinning sites has been observed previously for vortices driven along a single principle axis of periodic pinning arrays [34]. Additionally, a transition from a higher velocity random or turbulent type of vortex flow to a lower velocity flow state with smaller fluctuations was also observed in Ref. [34], a feature which resembles the transition in and out of the (1,0) step in figure 13(a). We find a very pronounced jump up in V_y at the end of each of the two locking steps which is correlated with a sudden jump in V_x (not shown).

Figure 13(b) shows that for $F_p = 2.5$, all the steps are gone and the flow is always in the strongly fluctuating regime. The former steps are replaced with local minima in V_y at the angles where the (0, 1), (1, 1), (1, 0), and $\theta = 90^\circ$ locking steps would have occurred, indicating that there is still a guidance effect from the substrate but not complete locking of the vortex motion. At $F_p = 2.75$ in figure 13(c), the (0,0), (1,1), and $\theta = 90^\circ$ locking steps reappear and a dip in V_y persists at $\theta = 60^\circ$ where the (1,0) step would have been. For $F_p = 2.75$, figure 13(d) shows that the (0,1), (1,2), (1,1), (2,1), and $\theta = 90^\circ$ steps are now all restored, while between the steps the flow enters a rapidly fluctuating phase in which V_y is significantly enhanced. In figure 13(d), along a given locking step V_y is not constant but has a curved shape and decreases noticeably just before the end of each step. The vortex flow on the steps occurs in the form of an incommensurate or solitonlike pulse of depinned vortices which passes through a

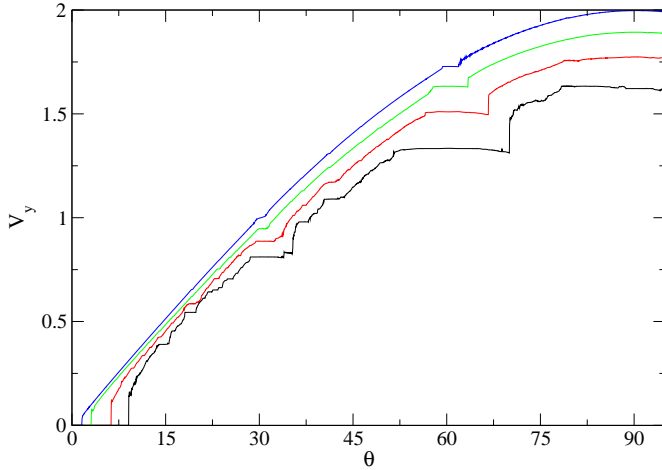


Figure 12. V_y vs θ for a triangular pinning array at $B/B_\phi = 1.11$ for different substrate strengths $F_p = 0.25, 0.5, 1.0,$ and 1.5 , from top to bottom. Here the step widths grow with increasing F_p .

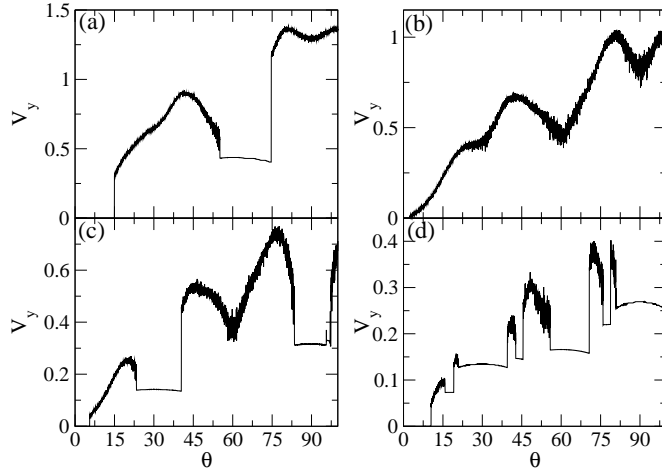


Figure 13. V_y vs θ for the sample from figure 12 with a triangular pinning array at $B/B_\phi = 1.11$. (a) $F_p = 2.35$. There are only two locking regions separated by strongly fluctuating regions where some guided motion of the particles occurs. (b) $F_p = 2.5$. The locking regions are almost completely absent. (c) $F_p = 2.75$. Several locking regions reappear. (d) $F_p = 2.85$. There are a larger number of locking steps interspersed with randomly fluctuating regions.

background of pinned vortices. For $F_p > 2.9$, the vortices transition directly from one locking step to the next locking step and there are no longer regions of random flow between the steps, as illustrated in figure 14 for a sample with $F_p = 3.0$ that exhibits a rich variety of locking steps. As F_p increases further, the V_y versus θ curves retain the shape shown in figure 14 with small shifts in the steps until $F_p \geq 3.9$, at which point all the vortices become pinned for all θ .

To demonstrate the differences in the flow for samples with strong and weak

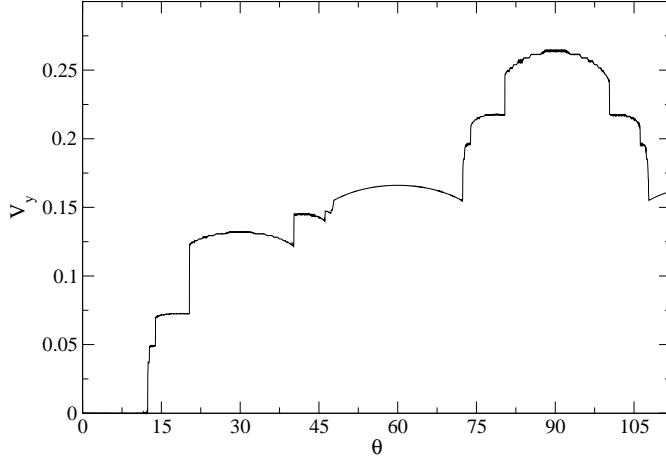


Figure 14. V_y vs θ for a triangular pinning array at $B/B_\phi = 1.11$ with $F_p = 3.0$. The random fluctuating regimes are lost and the system passes directly from one locking phase to the next.

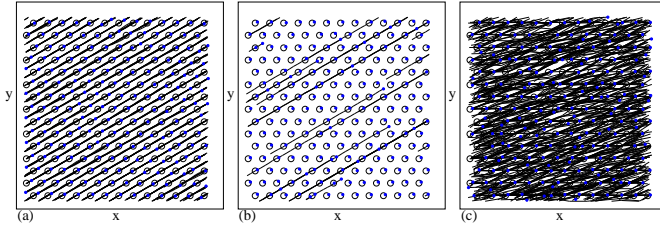


Figure 15. The positions of the pinning sites (large open circles) and vortices (small filled circles) as well as vortex trajectories over a fixed time interval (lines) in a portion of a sample with a triangular pinning array on the (1,1) locking step at $\theta = 30^\circ$. (a) In the weak pinning regime at $F_p = 1.75$, an ordered flow occurs with all the vortices moving along the $\theta = 30^\circ$ direction. (b) In the strong pinning regime at $F_p = 2.75$, a portion of the vortices are pinned and the flow occurs by a pulse motion or flowing kink. (c) At $F_p = 2.75$ for $\theta = 15^\circ$, a non-locking fluctuating flow phase occurs.

pinning, in figure 15(a,b) we plot the vortex trajectories on the (1,1) locking step at $\theta = 30^\circ$ over a fixed time interval. For $F_p = 1.75$, figure 15(a) shows that all the vortices move along one-dimensional paths oriented along the $\theta = 30^\circ$ driving direction. For $F_p = 2.75$ in figure 15(b), only a portion of the vortices move in one-dimensional paths along the pinning rows while the remaining vortices are pinned. Figure 15(c) shows that in the $F_p = 2.75$ sample at $\theta = 15^\circ$, a fluctuating flow phase occurs and there is no longer any one-dimensional channeling of the vortex motion. For samples with strong substrates, along the locking steps the vortices generally exhibit a triangular structure since a large portion of the vortices are trapped by the pinning sites, so the large scale structural transitions found for samples with weak substrates are lost. By conducting a series of simulations for varied F_p we map the transition between the strong and weak substrate regimes, as shown in figure 16 where we highlight the widths of the (0,1), (1,1), (1,0), and $\theta = 90^\circ$ locking steps.

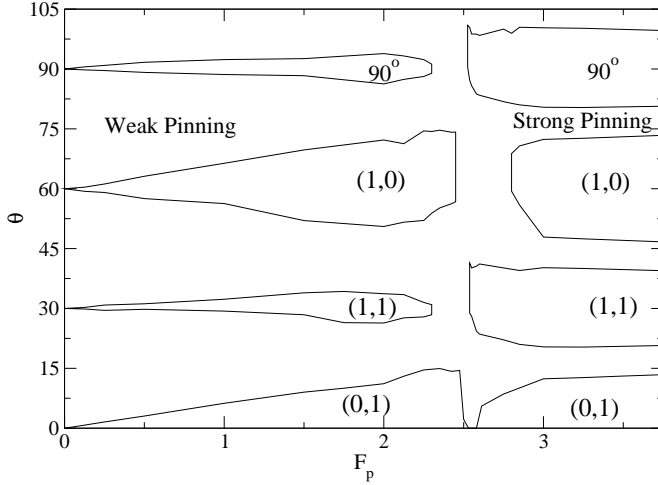


Figure 16. The dynamic phase diagram of θ vs F_p for a sample with a triangular pinning array at $B/B_\phi = 1.11$. The regions in which the (0,1), (1,1), (1,0), and 90° locking steps appear are marked. The left side of the diagram at lower F_p is the weak pinning regime. Near $F_p = 2.5$ a large portion of the vortex dynamics falls in the random fluctuating phase rather than on locking steps. In the strong pinning regime the second type of locking steps appear. For $F_p \geq 3.9$ all the vortices are pinned.

The (0,1) step increases in width with increasing F_p up to $F_p = 2.45$, after which the step vanishes. This denotes the transition from the weak pinning locking regime to the random fluctuating phase. For $F_p > 2.55$ the (0,1) step reappears in the strong pinning regime and its width saturates for $F_p > 3.0$. The higher order steps also show similar features with the step widths diminishing to zero at $F_p = 0.0$ and the steps vanishing close to $F_p = 2.5$. There are also many other higher order steps not shown in figure 16 which in general have similar behaviour.

In figure 17 we show that the crossover from the weak pinning to the strong pinning regime can also be identified by measuring P_6 versus F_p . We plot the width $\Delta\theta$ of the (1,0) step from figure 16 in figure 17(a), and show the corresponding P_6 in figure 17(b). At $F_p = 0.0$, $P_6 = 1.0$, and P_6 generally decreases with increasing F_p as more dislocations enter the system in the moving smectic phase until reaching $P_6 = 0.7$ at $F_p = 2.4$. There is then a dip in P_6 at $F_p = 2.5$ where the step width $\Delta\theta$ drops to zero. For $F_p > 2.5$, P_6 increases with increasing F_p until reaching $P_6 = 0.67$ when the system enters the strongly pinned regime and a large portion of the vortices become pinned in the triangular substrate, increasing the amount of sixfold ordering present. It is also possible to detect the crossover between the weak and strong pinning regimes using the average velocity in the y -direction V_y versus F_p for a given θ , as shown in Figure 18(a) for $\theta = 90^\circ$ and $\theta = 30^\circ$. At $F_p = 0.0$ the values of the velocities are simply $V_y = A \sin(30^\circ) = 1.0$ and $V_y = A \sin(90^\circ) = A = 2.0$. As F_p increases, V_y monotonically decreases until just above $F_p = 2.5$ which marks the crossover to the strong pinning regime in which V_y remains constant for increasing F_p . The decrease in V_y in the weak pinning regime can be fit to the functional form $V_y - V_y^c \propto (F_p - F_c^p)^\alpha$, where V_y^c is the saturation value of the velocity in the strong pinning regime and F_c^p is the critical value of the pinning force at which the system

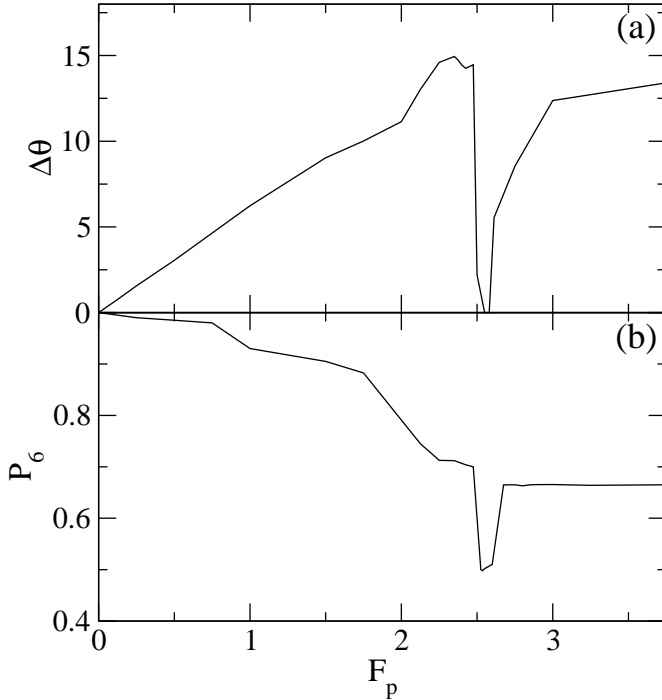


Figure 17. (a) The width $\Delta\theta$ of the $(1,0)$ locking phase from figure 16 vs F_p . (b) The corresponding fraction of six-fold coordinated particles P_6 has a dip in the random fluctuating phase which separates the weak and strong pinning regimes.

enters the strong pinning regime, identified as the value of F_p above which V_y becomes constant. In figure 18(b) we show this scaling with V_y normalized by $\sin(\theta)$. Here the $\theta = 30^\circ$ and $\theta = 90^\circ$ curves collapse on each other and the solid line indicates a fit with $\alpha = 1/3$. The behaviour of the V_y curves varies on different sets of locking steps, so a straightforward scaling such as that shown in figure 18(b) is not always possible. For example, in figure 19 we plot V_y versus F_p on the $(1,0)$ step as well as for a driving angle of $\theta = 17^\circ$. In both cases V_y decreases with increasing F_p for $F_p < 2.5$. For $\theta = 17^\circ$, V_y drops to zero within the weak pinning regime when the $(0,1)$ step widens to include this driving angle and the vortices move in one-dimensional channels that are aligned with the x axis. Near $F_p = 2.5$, V_y for both driving angles passes through a local maximum when the system enters the random fluctuating flow regime. At $F_p = 2.85$ for $\theta = 60^\circ$, the $(1,0)$ step reappears in the strong pinning regime, where V_y remains constant. Similarly for $\theta = 17^\circ$ V_y saturates to a nearly constant value in the strong pinning regime.

We next consider the effects of changing B/B_ϕ on the behaviour in the strong pinning regime. In figure 20 we plot V_y versus θ for a triangular pinning system with $F_p = 3.75$ at $B/B_\phi = 1.11, 1.48, 1.852, 2.407, 2.78, 3.148, 4.0,$ and 4.78 . The system is pinned at all θ for $B/B_\phi < 1.0$. For all of the fillings shown in figure 20, strong locking effects occur, and the widths of some of the locking steps vary with B/B_ϕ . For $B/B_\phi > 2.78$ the $(1,0)$ locking step shows increased curvature and regions of negative differential conductivity appear near $\theta = 38^\circ, 68^\circ,$ and 78° , while there is a dome like feature on the $\theta = 90^\circ$ locking step. At some values of B/B_ϕ , a series of smaller

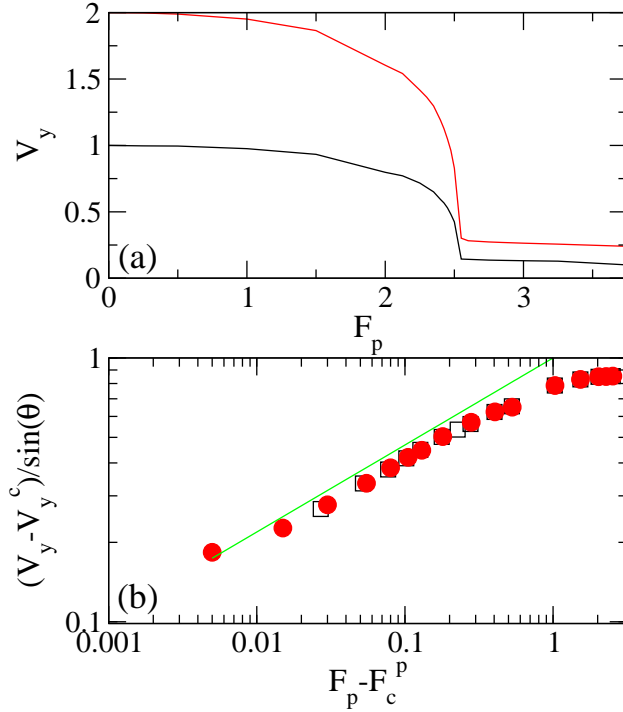


Figure 18. (a) The average velocity V_y vs F_p for the system in figure 16 at $\theta = 90^\circ$ (upper curve) and $\theta = 30^\circ$ (lower curve) showing that in the strong pinning regime the particle velocity saturates. (b) A scaling collapse of the same curves near the crossover at F_c^p from the weak pinning to the strong pinning regime. The line is a fit to $V_y - V_y^c \propto (F_p - F_c^p)^\alpha$ with $\alpha = 1/3$, where V_y^c is the value of the V_y in the strong pinning regime.

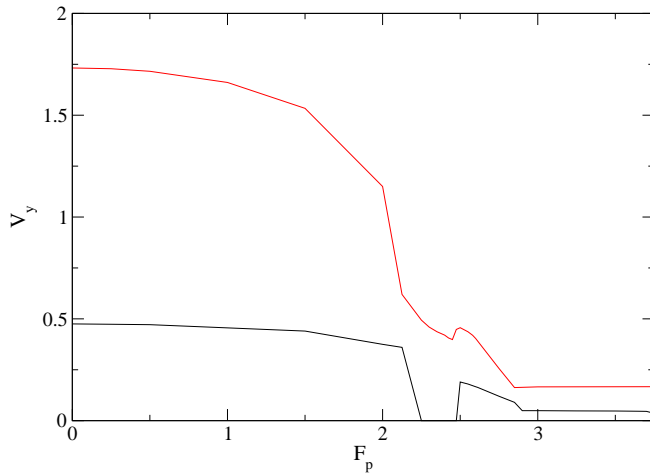


Figure 19. The average velocity V_y vs F_p for the system in figure 16 at $\theta = 60^\circ$ on the (1,0) step (upper curve) and at $\theta = 17^\circ$ (lower curve). Here a local maximum in V_y occurs in the random fluctuating regime which separates the weak and strong pinning regimes.

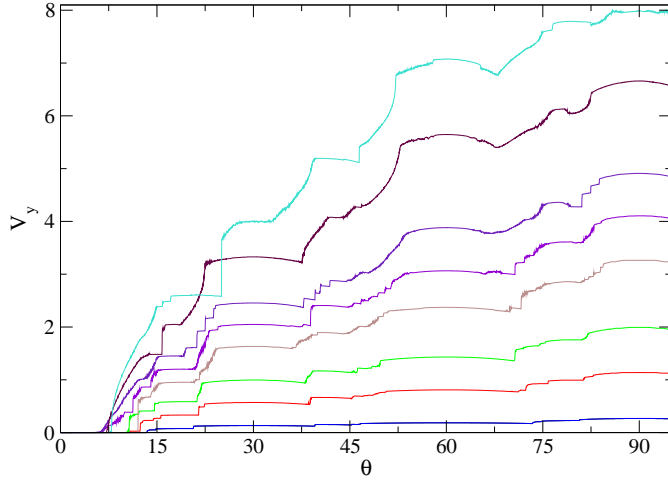


Figure 20. V_y vs θ for a triangular pinning array with $F_p = 3.75$ at $B/B_\phi = 1.11, 1.48, 1.852, 2.407, 2.78, 3.148, 4.0,$ and 4.78 , from bottom to top.

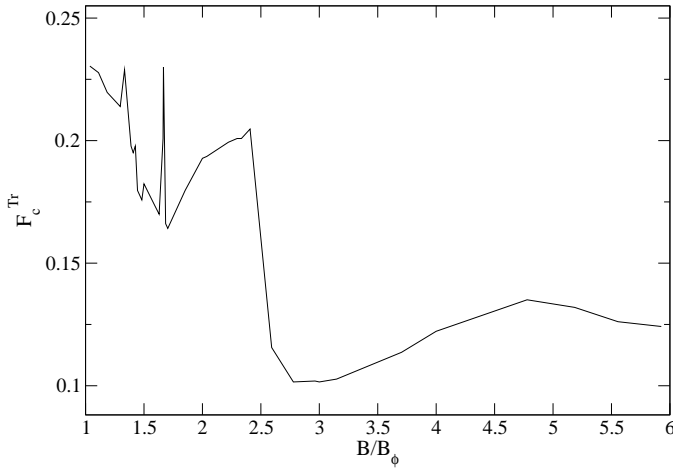


Figure 21. The width F_c^{Tr} of the $(0,0)$ step expressed in terms of the y component of the driving force at the end of the step vs B/B_ϕ for the triangular pinning system from figure 20.

locking steps appear, but these small steps disappear for larger values of B/B_ϕ . In general, all of the smaller steps are washed out for increasing B/B_ϕ .

In figure 21 we plot the width F_c^{Tr} of the $(0,0)$ step versus B/B_ϕ for the strong pinning regime sample from figure 20. The broad features of the curve are similar to the behaviour of F_c^{Tr} in the weak pinning regime that was shown in figure 6. There are several local minima and maxima in F_c^{Tr} and a broad maximum in the range $3.5 < B/B_\phi < 5.5$, as well as another local maximum near $B/B_\phi = 2.4$. As in the weak pinning regime, for the strong pinning regime the maxima in F_c^{Tr} are not centred at integer matching fields. Unlike the weak pinning regime, however,

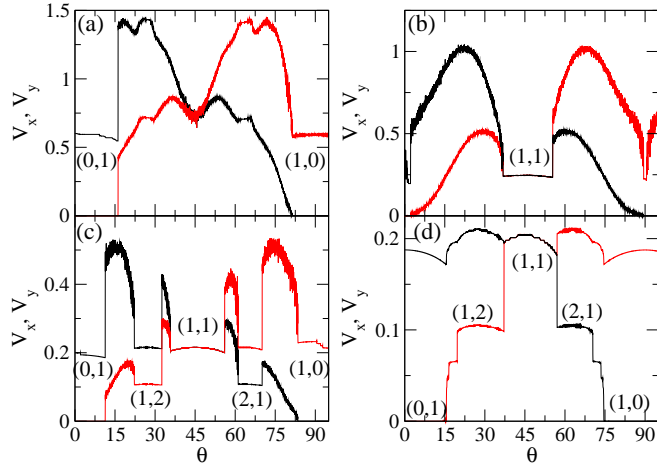


Figure 22. V_x (dark line) and V_y (light lines) vs θ for a sample with a square pinning array at $B/B_\phi = 1.11$. (a) At $F_p = 2.25$, only two locking steps are present which are separated by a random fluctuating phase. (b) At $F_p = 2.5$ the (1,1) locking step appears. (c) At $F_p = 2.75$ we find a mixture of locking steps and randomly fluctuating phases. (d) At $F_p = 3.75$ the system transitions directly from one locking step to another with no randomly fluctuating regimes.

there are no fillings at which F_c^{Tr} drops to zero. We also observe sharp and narrow peaks at $B/B_\phi = 4/3$ and $B/B_\phi = 5/3$, while no comparably sharp peaks in F_c^{Tr} occurred in the weak pinning regime. Longitudinal depinning studies performed for vortices moving over triangular pinning arrays have demonstrated enhanced pinning at fractional matching fields such as $B/B_\phi = 1/3$, $B/B_\phi = 2/3$, and higher order multiples where the vortices can form submatching configurations with triangular ordering [50]. The vortex flow on the (0,0) step for $B/B_\phi < 2.5$ occurs via the same flow of incommensurations along the pinning sites that was illustrated in figure 15(b), and the peaks in F_c^{Tr} at $B/B_\phi = 4/3$ and $B/B_\phi = 5/3$ correspond to fillings at which the moving incommensurations can form a triangular ordering. We expect that for a square pinning lattice in the strong pinning regime, peaks in the width of the first step would occur at $B/B_\phi = 3/2$, $5/4$, and $7/4$. In figure 21 for $B/B_\phi > 2.5$, a portion of the vortices begin to flow in the interstitial regions, which may prevent the formation of higher order fractional matching peaks.

We find the same transition from a weak pinning regime to a strong pinning regime for square pinning arrays. In figure 22(a) we plot V_x and V_y versus θ for a sample with square pinning at $F_p = 2.25$ and $B/B_\phi = 1.11$, where locking steps and randomly fluctuating phases appear. On the (0,1) and (1,0) locking steps, the vortices all flow along rows or columns of pinning sites. At $\theta = 45^\circ$ where the (1,1) step should appear, we find no step but instead both V_x and V_y pass through a local minimum. There are also some weak locking shoulder features in V_x and V_y near $\theta = 26^\circ$ and $\theta = 65^\circ$. Even though F_y reaches its maximum cycle value at $\theta = 90^\circ$, V_y sits in a local minimum at this driving angle. For $F_p = 2.5$ shown in figure 22(b), the (0,1) and (1,0) steps have almost completely disappeared; however, there is now a clear (1,1) locking step. At $F_p = 2.75$, figure 22(c) indicates that locking steps emerge at (0,1), (1,2), (1,1), (2,1), and (1,0), with large fluctuating regions falling between adjacent

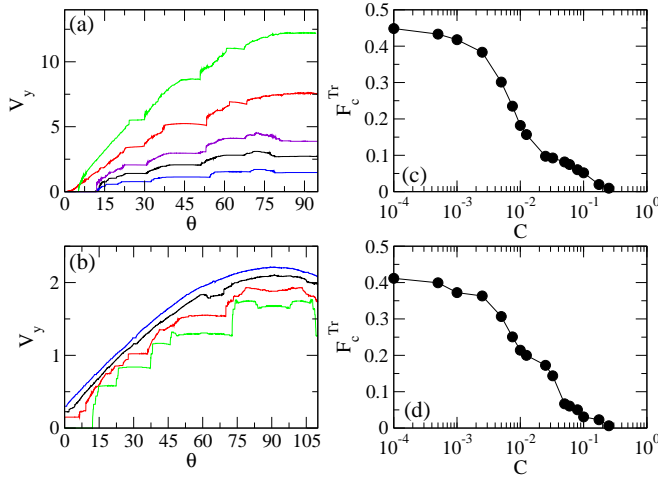


Figure 23. (a) V_y vs θ for colloidal particles with interaction strength $C = 0.001$ on a square pinning array with $F_p = 1.85$. The ratio of the number of colloids to pinning sites is $N_c/N_p = 0.432, 0.778, 1.125, 1.82,$ and 2.85 , from bottom to top. (b) V_y vs θ for colloidal particles on a triangular pinning array with $F_p = 1.85$ for $N_c/N_p = 0.432$ and varied colloid-colloid interaction strength of $C = 0.0001, 0.01, 0.05,$ and 0.1 , from bottom to top. (c) The width F_c^{Tr} of the first locking step from the square pinning array sample in panel (a) at $N_c/N_p = 0.432$ vs C . (d) The same as (c) for a triangular pinning array with the same parameters as in panel (b).

locking steps. For $F_p > 3.0$ the system enters the strong pinning regime and the random fluctuating regions disappear, as shown in figure 22(d) for $F_p = 3.75$. Here, V_y is higher on the (2,1) step than on the (1,0) step even though no random fluctuating region separates the two steps. The length of the moving incommensurations on the (2,1) step is slightly larger than the length of the moving incommensurations along the (1,0) step, leading to the higher value of V_y for the (2,1) step.

7. Colloidal Particles Moving Over Triangular and Square substrates

Another question is how general the results we have obtained for the vortex system are for other types of particle interactions, particularly colloidal particles where there is currently considerable interest in kinetic locking effects. We have tested all of the major predictions for the vortex system on square and triangular pinning lattices for colloidal particles interacting with a screened Yukawa potential. In figure 23(a) we plot V_y vs θ for colloidal particles on a square pinning array of strength $F_p = 1.85$ for varied colloid densities of $N_c/N_p = 0.432, 0.778, 1.125, 1.82,$ and 2.85 . The colloid-colloid interaction coefficient is $C = 0.001$. Here we find the same locking step features observed for the vortex system, with the same oscillations in the width of the first and higher order steps. At $N_c/N_p = 1.82$ the width of the first step drops to zero, but the first step reappears at $N_c/N_p = 2.85$, similar to what was observed for the vortex system. We also find the same behaviours for colloids on triangular pinning arrays. One quantity that can be varied in the colloidal system but not in the vortex system is the particle-particle interaction strength. This can be achieved either by increasing

the effective charge of the colloids or by changing the screening length while keeping the strength of the substrate fixed. In figure 23(b) we plot V_y versus θ for colloids on a triangular pinning lattice at fixed $F_p = 1.85$ and $N_c/N_p = 0.432$ with $C = 0.0001, 0.01, 0.05,$ and 0.1 . As C increases, the widths of the locking steps decrease since the colloid lattice becomes stiffer and is less able to distort to adjust to the pinning.

Figure 23(d) shows the width F_c^{Tr} of the first locking step as given by the value of the y component of the driving force at the end of the step as a function of C for colloids on a triangular pinning lattice from the system in figure 23(b). As C increases, F_c^{Tr} gradually decreases to zero. There is no clear transition between weak and strong pinning regimes when C is varied, unlike the transition found when F_p was varied for the vortex system. This is because our choice of fixed $F_p = 1.85$ falls below the driving amplitude of $A = 2.0$, so all the colloids are moving even when the particle-particle interaction strength is negligible. In order to observe the strong pinning regime discussed earlier, it is necessary for a portion of the particles to be pinned and for the motion to occur in the form of depinned incommensurations which pass through the system. In figure 23(c) we plot the width F_c^{Tr} of the first locking step versus C for colloids on a square pinning array with the same parameters used in figure 23(a), indicating that the same behaviour found for colloids on a triangular pinning lattice also occurs for colloids on a square pinning lattice.

8. Summary

In summary, we have investigated the collective ordering and disordering effects on directional locking for particles such as vortices and colloids moving over triangular and square substrate arrays. We identify several different regimes of collective behaviour as a function of the substrate strength and of the ratio of particle density to substrate minima density. For weak substrates, at certain driving angles all the particles flow along one-dimensional channels through the pinning sites, generating a series of constant velocity steps on which the motion remains locked to a certain direction over a range of driving angles. As the pinning strength decreases, the width of the locking steps decreases and larger ranges of driving angle are occupied by nonlocking regions in which the particle-particle interactions dominate and a triangular particle lattice forms. On the locking steps for triangular substrate arrays, we find that a rich variety of different types of moving lattices form, including moving smectic, square, anisotropic disordered, and distorted triangular lattice structures. The most prominent locking steps are associated with smectic type particle orderings. In the weak substrate regime, we observe that the widths of the steps including the initial transverse depinning barrier pass through local minima and maxima as a function of the ratio of particle density to substrate minima density. In contrast to the longitudinal depinning threshold for periodic substrates, which shows peaks at commensurate fields, the local maxima for the width of the first locking step are not correlated with the two-dimensional periodicity of the pinning array but are instead related to a dynamical commensuration effect caused by the formation of one-dimensional channels of moving particles. A local maximum in the width of the first locking step occurs when integer numbers of rows of moving vortices can fit in the interstitial areas between the pinning sites. For fillings at which the moving rows are unable to fit without buckling, the particle structure becomes disordered and the width of the first locking step is small or zero. As a function of substrate strength for fixed particle density, we identify two distinct locking regimes: a weak pinning regime where all the particles flow along

the pinning sites, and a strong pinning regime where the flow occurs by means of an incommensuration or a pulse passing through a background of pinned particles. Between these two regimes the locking steps are lost and are replaced by a strongly fluctuating regime where the particle motion does not lock to a particular direction. For a fixed driving angle, the average particle velocity drops sharply at the crossover between these two regimes, and the velocity saturates to a plateau value in the strong substrate limit. In the strong substrate regime the width of the first step displays commensurate peaks when the number of particles is a fractional matching ratio of the number of substrate minima, in addition to showing peaks at the incommensurate fields as in the weak pinning regime. We expect these effects to be relevant to a wide class of collectively interacting particles moving over periodic substrates, such as vortices in type II superconductors, colloids, electron crystals, and other soft matter systems.

9. Acknowledgments

This work was supported by the U.S. Department of Energy under Contract No. W-7405-ENG-36.

References

- [1] Reichhardt C and Nori F 1999 *Phys. Rev. Lett.* **82** 414
- [2] Wiersig J and Ahn K-H 2001 *Phys. Rev. Lett.* **87** 026803
- [3] Korda P T, Taylor M B and Grier D G 2002 *Phys. Rev. Lett.* **89** 128301
- [4] MacDonald M P, Spalding G C and Dholakia K 2003 *Nature (London)* **426** 421
- [5] Lacasta A M, Sancho J M, Romero A H and Lindenberg K 2005 *Phys. Rev. Lett.* **94** 160601
Gleeson J P, Sancho J M, Lacasta A M and Lindenberg K 2006 *Phys. Rev. E* **73** 041102
Sancho J M and Lacasta A M 2010 *Eur. Phys. J. Special Topics* **187** 49
- [6] Reichhardt C and Olson Reichhardt C J 2004 *Phys. Rev. E* **69** 041405
- [7] Gopinathan A and Grier D G 2004 *Phys. Rev. Lett.* **92** 130602
- [8] Pelton M, Ladavac K and Grier D G 2004 *Phys. Rev. E* **70** 031108
Roichman Y, Wong V and Grier D G 2007 *Phys. Rev. E* **75** 011407
- [9] Long B R, Heller M, Beech J P, Linke H, Bruus H and Tegenfeldt J O 2008 *Phys. Rev. E* **78** 046304
- [10] Speer D, Eichhorn R and Reimann P 2010 *Phys. Rev. Lett.* **105** 090602
- [11] Speer D, Eichhorn R and Reimann P 2009 *Phys. Rev. Lett.* **102** 124101
- [12] Frechette J and Drazer G 2009 *J. Fluid Mech.* **627** 379
- [13] Balvin M, Sohn E, Iracki T, Drazer G and Frechette J 2009 *Phys. Rev. Lett.* **103** 078301
- [14] Herrmann J, Karweit M and Drazer G 2009 *Phys. Rev. E* **79** 061404
- [15] Xiao K and Grier D G 2010 *Phys. Rev. Lett.* **104** 028302
Xiao K and Grier D G 2010 *Phys. Rev. E* **82** 051407
- [16] Khoury M, Lacasta A M, Sancho J M, Romero A H and Lindenberg K 2008 *Phys. Rev. B* **78** 155433
- [17] Louthback K, Puchalla J, Austin R H and Sturm J C 2009 *Phys. Rev. Lett.* **102** 045301
Louthback K, Chou K S, Newman J, Puchalla J, Austin R H and Sturm J C 2010 *Microfluidics Nanofluidics* **9** 1143
- [18] Huang L R, Cox E C, Austin R H and Sturm J C 2004 *Science* **304** 987
- [19] Reichhardt C, Olson C J and Hastings M B 2002 *Phys. Rev. Lett.* **89** 024101
Reichhardt C and Olson Reichhardt C J 2003 *Phys. Rev. E* **68** 046102
- [20] Tierno P, Johansen T H and Fischer T M 2007 *Phys. Rev. Lett.* **99** 038303
Soba A, Tierno P, Fischer T M and Sagues F 2008 *Phys. Rev. E* **77** 060401(R)
- [21] Koplík J and Drazer G 2010 *Phys. Fluids* **22** 052005
- [22] Marconi V I, Candia S, Balenzuela P, Pastoriza H, Domínguez D and Martinoli P 2000 *Phys. Rev. B* **62** 4096
- [23] Carneiro G 2002 *Phys. Rev. B* **66** 054523

- [24] Surdeanu R, Wijngaarden R J, Griessen R, Einfeld J and Wördenweber R 2001 *Europhys. Lett.* **54** 682
- [25] Silhanek A V, Van Look L, Raedts S, Jonckee R and Moshchalkov V V 2003 *Phys. Rev. B* **68**, 214504
- [26] Villegas J E, Gonzalez E M, Montero M I, Schuller I K and Vicent J L 2003 *Phys. Rev. B* **68** 224504
- [27] Giamarchi T and Le Doussal P 1996 *Phys. Rev. Lett.* **76** 3408
- [28] Reichhardt C and Olson Reichhardt C J 2007 *Phys. Rev. B* **76** 214305
- [29] Achim C V, Ramos J A P, Karttunen M, Elder K R, Granato E, Ala-Nissila T and Ying S C 2009 *Phys. Rev. E* **79** 011606
- [30] Yang Y, Duan W-S, Chen J-M, Yang L, Tekić J, Shao Z-G and Wang C-L 2010 *Phys. Rev. E* **82** 051119
- [31] Granato E and Ying S C 2000 *Phys. Rev. Lett.* **85** 5368
- [32] Reichhardt C and Olson Reichhardt C J 2011 *Phys. Rev. Lett.* **106** 060603
- [33] Harada K, Kamimura O, Kasai H, Matsuda T, Tonomura A and Moshchalkov V V 1996 *Science* **274** 1167
- [34] Reichhardt C, Olson C J and Nori F 1998 *Phys. Rev. B* **57** 7937
- [35] Berdiyrov G R, Milosevic M V and Peeters F M 2006 *Phys. Rev. B* **74** 174512
- [36] Reichhardt C, Olson C J and Nori F 1997 *Phys. Rev. Lett.* **78** 2648
Reichhardt C, Zimányi G T and Grønbech-Jensen N 2001 *Phys. Rev. B* **64** 014501
- [37] Reichhardt C and Olson Reichhardt C J 2008 *Phys. Rev. B* **78** 180507(R)
- [38] Moon K, Scalettar R T and Zimányi G T 1996 *Phys. Rev. Lett.* **77** 2778
Olson C J, Reichhardt C and Nori F 1998 *Phys. Rev. Lett.* **81** 3757
Kolton A B, Domínguez D and Grønbech-Jensen N 1999 *Phys. Rev. Lett.* **83** 3061
- [39] Le Doussal P and Giamarchi T 1998 *Phys. Rev. B* **57** 11356
Balents L, Marchetti M C and Radzihovsky L 1998 *Phys. Rev. B* **57** 7705
- [40] Pardo F, de la Cruz F, Gammel P L, Bucher E and Bishop D J 1998 *Nature (London)* **396** 348
- [41] Fangohr H, Cox S J and de Groot P A J 2001 *Phys. Rev. B* **64** 064505
- [42] Fangohr H, de Groot P A J and Cox S J 2001 *Phys. Rev. B* **63** 064501
- [43] Reichhardt C and Zimanyi G T 2000 *Phys. Rev. B* **61** 14354
- [44] Carneiro G 2002 *Phys. Rev. B* **66** 054523
- [45] Gutierrez J, Silhanek A V, Van de Vondel J, Gillijns W and Moshchalkov V V 2009 *Phys. Rev. B* **80** 140514(R)
Avci S, Xiao Z L, Hua J, Imre A, Divan R, Pearson J, Welp U, Kwok W K and Crabtree G W 2010 *Appl. Phys. Lett.* **97** 042511
- [46] Olson Reichhardt C J and Reichhardt C 2009 *EPL* **88** 47004
- [47] Fiory A T, Hebard A F and Somekh S 1978 *Appl. Phys. Lett.* **32** 73
Baert M, Metlushko V V, Jonckheere R, Moshchalkov V V and Bruynseraede Y 1995 *Phys. Rev. Lett.* **74** 3269
Martín J I, Vélez M, Nogués J and Schuller I K 2002 *Phys. Rev. Lett.* **79** 1929
Welp U, Xiao Z L, Jiang J S, Vlasko-Vlasov V K, Bader S D, Crabtree G W, Liang J, Chik H and Xu J M 2002 *Phys. Rev. B* **66** 212507
- [48] Anders S, Smith A W, Besseling R, Kes P H and Jaeger H M 2000 *Phys. Rev. B* **62** 15195
Besseling R, Kes P H, Dröse T and Vinokur V M 2005 *New J. Phys.* **7** 71
- [49] Karapetrov G, Fedor J, Iavarone M, Rosenmann D and Kwok W K 2005 *Phys. Rev. Lett.* **95** 167002 (2005).
- [50] Reichhardt C and Grønbech-Jensen N 2001 *Phys. Rev. B* **63** 054510
Ooi S, Mochiku T and Hirata K 2009 *J. Phys.: Conf. Ser.* **150** 052203